ISSN 1063-7834, Physics of the Solid State, 2016, Vol. 58, No. 10, pp. 1981–1988. © Pleiades Publishing, Ltd., 2016.
Original Russian Text © T.V. Drokina, G.A. Petrakovskii, O.A. Bayukov, A.M. Vorotynov, D.A. Velikanov, M.S. Molokeev, 2016, published in Fizika Tverdogo Tela, 2016, Vol. 58, No. 10, pp. 1913–1920.

MAGNETISM

Synthesis and Structural, Magnetic, and Resonance Properties of the $LiCuFe_2(VO_4)_3$ Compound

T. V. Drokina[a]*, G. A. Petrakovskii[a], O. A. Bayukov[a], A. M. Vorotynov[a], D. A. Velikanov[a], and M. S. Molokeev [a, b]

[a] *Kirensky Institute of Physics, Siberian Branch, Russian Academy of Sciences, Akademgorodok 50, building 38, Krasnoyarsk, 660036 Russia*

[b] *Far Eastern State Transport University, ul. Serysheva 47, Khabarovsk, 680000 Russia*

**e-mail: tvd@iph.krasn.ru*

Received March 10, 2016

Abstract—Complex studies have been performed for the structural, static magnetic, and resonance properties of a new magnet $LiCuFe_2(VO_4)_3$ prepared by solid-phase synthesis. The temperature dependence of the susceptibility has an anomaly at temperature $T_{max} = 9.6$ K. At high temperatures, the $LiCuFe_2(VO_4)_3$ sample is in the paramagnetic state described by the Curie–Weiss law at $T > 50$ K and mainly determined by iron ions with effective magnetic moment $\mu_{eff(exp)} = 8.6\mu_B$ per formula unit. At low temperatures, a long-range magnetic order is observed in the magnetic subsystem of the sample; the order is predominantly characterized by the antiferromagnetic exchange interaction and high frustration level. The exchange interaction parameters are estimated in a six-sublattice representation of the $LiCuFe_2(VO_4)_3$ magnet. It is shown that the $LiCuFe_2(VO_4)_3$ compound is an antiferromagnet with strong intrachain and frustrating interchain exchange interactions.

DOI: 10.1134/S1063783416100139

1. INTRODUCTION

The interest to magnets with competing exchange interactions increases in relation to searching for new functional materials for spintronics. The exchange interaction frustrations which can form in these compounds can lead to formation of unusual magnetic structures [1–3] that attract the attention of researchers due to interesting static and dynamic properties and opening perspectives of new practical applications. For example, the formation of a collective magnetic spin ice state was observed in frustrated compounds with the pyrochlorine crystal lattice [1, 4, 5]. The study of the properties of new compounds with competing exchange interactions and complex spin architecture is a topical problem of the contemporary physics of condensed state.

Multicomponent vanadates, among them those with general formula $ABFe_2(VO_4)_3$, where A are univalent alkali-earth elements and B are bivalent elements (Cu^{2+}), are oxide compounds with complex magnetic and anion structures and can be the base of searching for new materials with competing exchange interactions.

The X-ray diffraction study of the $LiCuFe_2(VO_4)_3$ inorganic compound [6] showed that, at room temperature, the crystal structure was described by triclinic space symmetry group $P\bar{1}$. The unit cell includes two formula units ($Z = 2$).

The specific features of the crystal structure of the $LiCuFe_2(VO_4)_3$ compound and the existence of two magnetic ions (Cu^{2+} and Fe^{3+}) occupying the nonequivalent crystallographic positions, allow one to assume the existence of competing exchange interactions and, as a result, the unpredicted magnetic properties. This was an impetus to studying vanadate $LiCuFe_2(VO_4)_3$.

This paper presents the results of the X-ray diffraction, magnetic, and resonance measurements of the $LiCuFe_2(VO_4)_3$ compound.

2. SAMPLE SYNTHESIS AND EXPERIMENTAL TECHNIQUE

$LiCuFe_2(VO_4)_3$ samples were prepared by solid-phase synthesis from the mixture of oxides Fe_2O_3, Li_2CO_3, CuO, and V_2O_5 taken according to the compound stoichiometry with annealing for two stages (with intermediate milling) at temperatures $T_1 = 650°C$, $T_2 = 680°C$ and holding tomes $\tau_1 = \tau_2 = 24$ h in air. The chemical and the phase compositions of the samples were controlled using the X-ray diffraction.

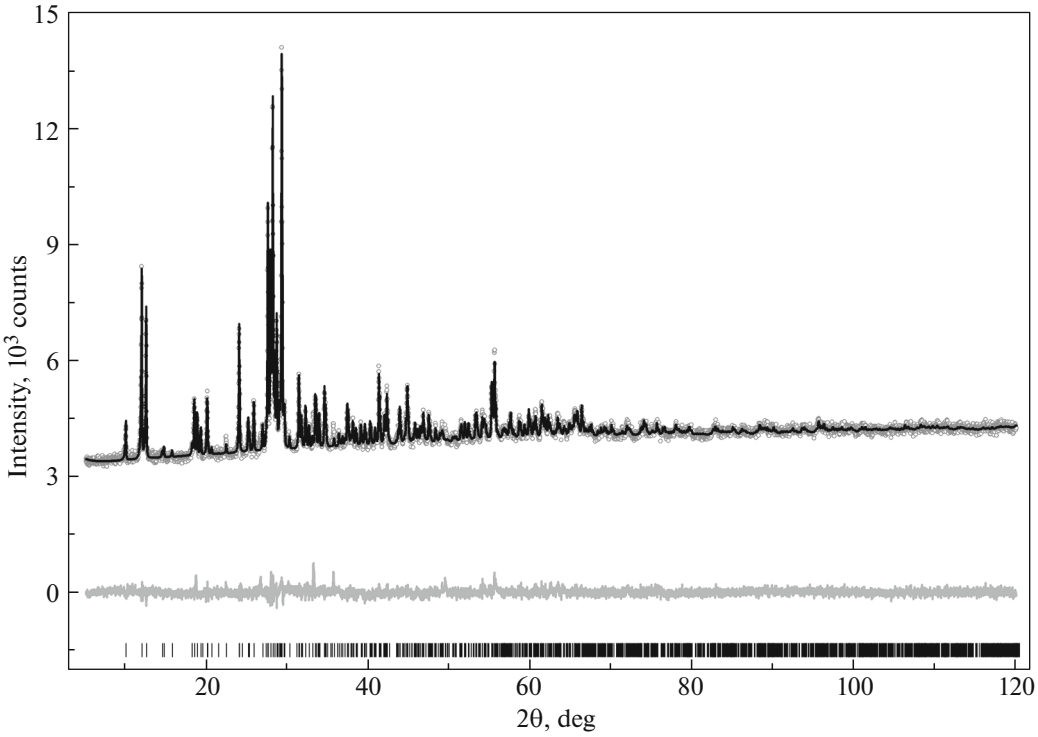

Fig. 1. X-ray diffraction pattern of the polycrystalline $LiCuFe_2(VO_4)_3$ compound measured at temperature $T = 300$ K.

The X-ray powder diffraction pattern of the $LiCuFe_2(VO_4)_3$ polycrystalline sample at room temperature was obtained using a Bruker D8 ADVANCE diffractometer with a VANTEC linear detector and CuK_α radiation. The scanning pitch in angle 2θ was 0.016°, the exposition was 0.6 s a pitch.

The static magnetic characteristics of the samples were measured in the temperature range 4–300 K in magnetic field $H = 0.05$ T using a SQUID magnetometer designed at the Kirensky Institute of Physics, Siberian Branch, RAS [7].

The electron magnetic resonance spectra were measured in the *X* diapason in the temperature range 110–300 K using a Bruker Elexsys E580. The spectra were recorded using the following parameters: the microwave power was 0.63 mW, the modulation amplitude was 0.7 G, the modulation frequency was 100 kHz, the sweep width of magnetic field 5000 G, and the sweep time was 40 s.

The nuclear gamma-resonance spectra were measured on powders 5–10 mg/cm^2 in thickness in the natural iron content at room temperature using a MS-1104Em spectrometer designed at the Kirensky Institute of Physics, Siberian Branch of RAS and a Co^{57} (Cr) source. The chemical shifts are given with respect to α-Fe.

3. EXPERIMENTAL RESULTS

3.1. Data of Structural Studies

Figure 1 shows the X-ray powder of the $LiCuFe_2(VO_4)_3$ compound measured at room temperature. According to the X-ray diffraction data, the synthesized samples were single-phase and the X-ray diffraction pattern does not contain reflections corresponding to impurity phases. Since the structure of the $LiCuFe_2(VO_4)_3$ compound was determined in [6], it was used as initial Rietveld refinement model in the TOPAS 4.2 [8]. The refinement occurred stably and gave low factors of doubtfulness (Table 1). Table 2 lists the atomic coordinates and the thermal parameters of $LiCuFe_2(VO_4)_3$. Note that the unit cell parameters of the sample under study (Table 1) are close to the data obtained in [6]: $a = 8.1484(5)$ Å, $b = 9.8024(7)$ Å, $c = 6.6355(4)$ Å, $\alpha = 103.832(3)°$, $\beta = 102.353(3)°$, and $\gamma = 106.975(3)°$.

Figure 2a shows the crystal structure of the $LiCuFe_2(VO_4)_3$ compound. According to the data of [6] and our X-ray diffraction studies of the sample synthesized, Fe^{3+} ions in the $LiCuFe_2(VO_4)_3$ crystal were in the octahedral oxygen environment an occupied two crystallographically nonequivalent positions in the unit cell: Fe(1) and Fe(2). Two $Fe(1)O_6$ octahedra had a common edge, thus forming dimers. The dimers of $Fe(2)O_6$ octahedra form similarly. The bivalent copper ions were in an oxygen environment that

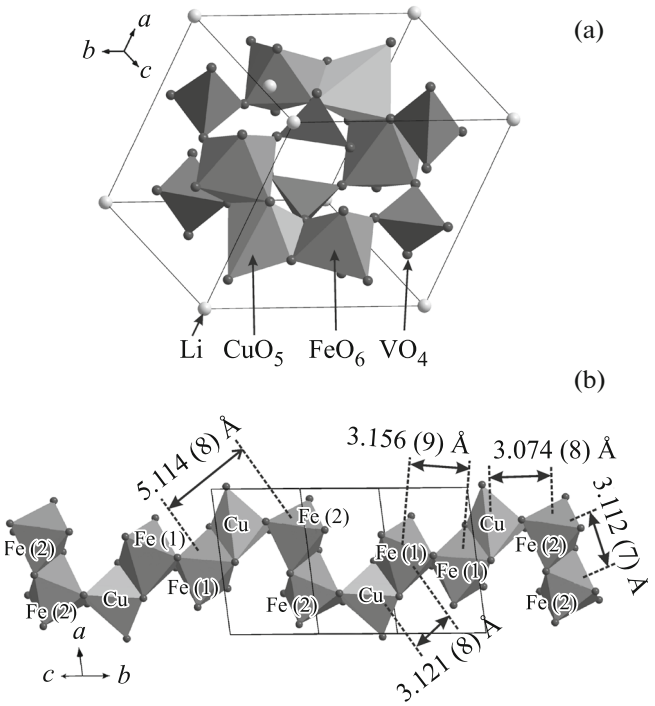

Fig. 2. (a) Crystal structure of the $LiCuFe_2(VO_4)_3$ compound and (b) the ...–Fe(2)–Fe(2)–Cu–Fe(1)–Fe(1)–Cu–Fe(2)–Fe(2)–... chain with characteristic interatomic distances.

forms CuO_5 trigonal bipyramids. The dimmers had common edges with CuO_5 polyhedra and were aligned in chains elongated along the **b**–**c** direction (Fig. 2b). In turn, the dimer clusters were surrounded by VO_4 tetrahedra; in this case, the $Fe(1)_2V_8$ and $Fe(2)_2V_{10}$ complexes forming the $[Fe_4V_6O_{24}]_\infty$ three-dimensional structure (skeleton] form. The voids of this skeleton contain Li ions: the $Li(1)O_6$ and $Li(2)O_{10}$ formations connected via the common face form infinite zigzag-shaped chains along the **b**–**c** direction.

Table 1. Main parameters of the X-ray diffraction experiment and the results of refinement of the crystal structure of the $LiCuFe_2(VO_4)_3$ compound (space group $P\bar{1}$) at room temperature

Parameter	Value
a, Å	8.1489(2)
b, Å	9.8047(2)
c, Å	6.6341(1)
α, deg	103.811(2)
β, deg	102.370(2)
γ, deg	106.975(2)
V, Å	468.74(2)
Angular range 2θ, deg	5–120
Number of reflections	1406
Number of refined parameters	92
R_{wp}, %	1.99
R_p, %	1.51
R_B, %	0.78
χ^2	1.29

Note: a, b, c, α, β, γ are unit cell parameters; V is unit cell volume, the reliability factors: R_{wp} is the weight profile factor, R_p is the profile factor, R_B is the integral factor; χ^2 is the fitting quality.

To estimate the iron state in $LiCuFe_2(VO_4)_3$, the Mössbauer spectrum study was performed. At room temperature, the Mössbauer spectrum was a sum of quadrupole doublets with various intensities (Fig. 3a). The interpretation of the spectrum was carried out for two stages. At the first stage, the distribution of quadrupole splitting P(QS) in the experimental spectrum was determined (Fig. 3b). The distribution was obtained by fitting of two groups of seed doublets with different chemical shifts. The maxima and peculiarities in distribution P(QS) demonstrate the existence of possible nonequivalent positions of iron in the sample. At the second stage of the interpretation, the model spectrum built on the base of information obtained from P(QS)was fitted to the experimental spectrum when varying all parameters of the hyperfine structure. The interpretation results are given in Table 3.

The chemical shifts corresponded to iron cations existed in trivalent (Fe^{3+}) and high-spin (S = 5/2) states. The Mössbauer positions were assigned to the crystallographic position by comparing the quadrupole splitting and the gradient of the electric field induced by the oxygen polyhedron and calculated

Table 2. Atomic coordinates, isotropic thermal parameters B_{iso} and population of the crystal structure of the $LiCuFe_2(VO_4)_3$ compound at temperature T = 300 K

Atom	x/a	y/b	z/c	B_{iso}, Å^2	Population
Cu	0.7854(10)	0.2932(8)	0.2696(12)	0.7(3)	1
Fe(1)	0.4487(12)	0.1086(10)	0.3838(17)	0.2(3)	1
Fe(2)	0.7025(11)	0.5146(9)	0.0411(15)	0.2(2)	1
V(1)	0.6051(12)	0.8407(10)	0.1201(18)	0.9(3)	1
V(2)	0.2306(11)	0.3754(9)	0.4097(15)	0.8(3)	1
V(3)	0.1608(11)	0.7706(9)	0.2225(15)	0.5(3)	1
Li(1)	0	0	0	2	1
Li(2)	0.03(3)	0.00(4)	0.48(5)	2	0.5
O(1)	0.016(4)	0.241(3)	0.298(5)	2	1
O(2)	0.524(4)	−0.090(3)	0.334(5)	2	1
O(3)	0.293(4)	0.489(3)	0.249(5)	2	1
O(4)	0.334(4)	0.247(3)	0.429(5)	2	1
O(5)	0.245(4)	0.755(3)	0.483(6)	2	1
O(6)	0.585(3)	0.648(3)	0.085(4)	2	1
O(7)	0.828(4)	−0.075(3)	0.154(4)	2	1
O(8)	0.510(4)	0.143(3)	0.124(6)	2	1
O(9)	0.774(4)	0.341(3)	0.006(5)	2	1
O(10)	0.716(4)	0.493(3)	0.341(5)	2	1
O(11)	0.177(4)	−0.043(3)	0.231(4)	2	1
O(12)	−0.061(4)	0.674(3)	0.184(5)	2	1

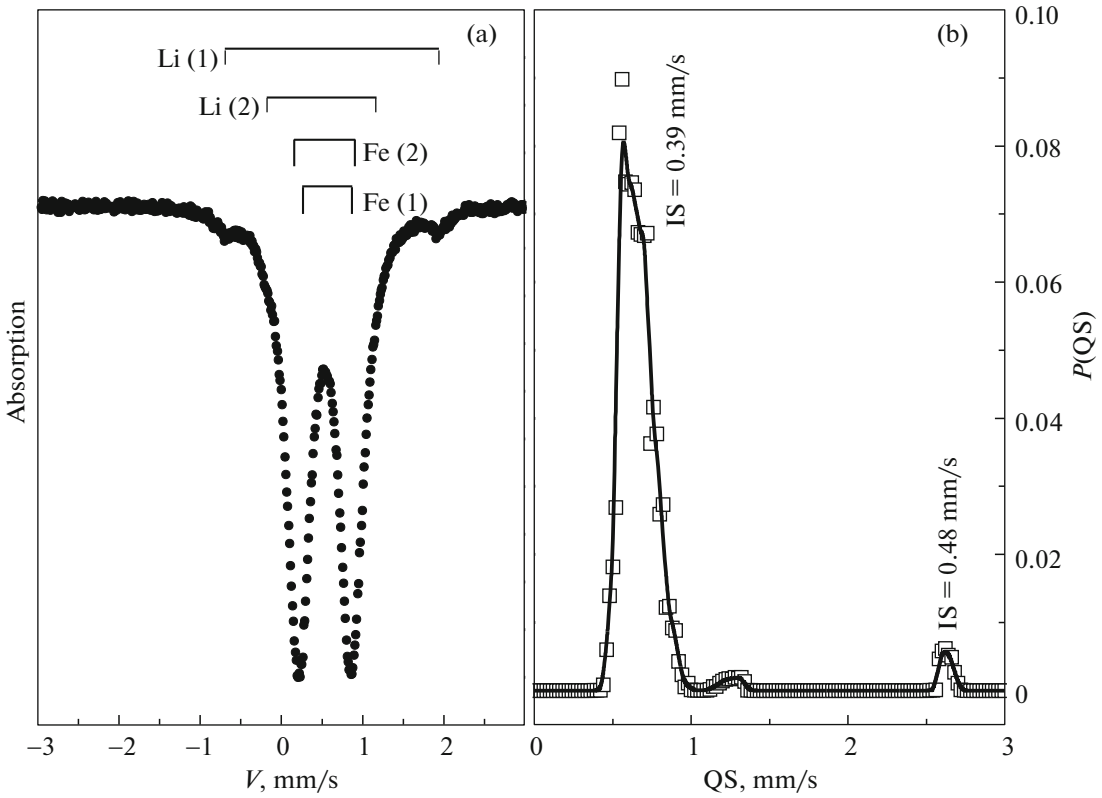

Fig. 3. (a) Mössbauer spectrum of $LiCuFe_2(VO_4)_3$ measured at room temperature and (b) the distribution of probability of quadrupole splitting in it.

based on the X-ray diffraction data in the framework of the point charge model. Along main Fe(1) and Fe(2) positions, the spectrum contained a small amount (~2%) of additional iron positions. The chemical shifts of these position corresponded to a relatively large coordination number in oxygen (6 and larger). These positions possibly belong to the iron atoms occupying lithium positions in the lattice. It is not inconceivable that they can be assigned to the interstitial introduction cations.

3.2. Results of Resonance Studies

To characterize the properties of the $LiCuFe_2(VO_4)_3$ material, we also used the results of the measurements using the electron paramagnetic resonance (EPR) method. The studies showed that the EPR signal measured on the $LiCuFe_2(VO_4)_3$ compound in the *X* diapason in the temperature range 110–300 K was an Lorentzian individual resonance line. Figure 4a illustrates the EPR spectrum measured at a temperature of 300 K. The main parameters of the observed first derivative of the absorption EPR signal had the following values: the resonance field (field corresponding to the intersection of the contour of derivative $d\chi''/dH$ with the zero line) was H_{res} = 3376 Oe and the line width (the distance in field between the extremes in the curve of the absorption line derivative) was ΔH = 846 Oe. Figures 4b–4d depict the results of studying the temperature dependences of amplitude *A* (the distance between extremes in the $d\chi''/dH$ along the ordinate axis), resonance field H_{res}, and width ΔH of the observed absorption EPR derivative line. It is seen that the resonance field was unchanged in the temperature range 110–300 K (Fig. 4c). As temperature decreased, the magnetic resonance signal line increased monotonically (Fig. 4d), which could be due to the increase in the local fields at magnetic ions of the sample.

Table 3. Mössbauer parameters of $LiCuFe_2(VO_4)_3$

IS, mm/s (±0.05)	QS, mm/s (±0.02)	*W*, mm/s (±0.02)	*A* (±0.03)	$\lvert V_{zz}\rvert$, $e/Å^3$	Position
0.380	0.55	0.27	0.43	0.408	Fe(1)
0.381	0.75	0.31	0.53	1.150	Fe(2)
0.315	1.29	0.18	0.02	0.234	Li(2)
0.472	2.63	0.20	0.02	0.604	Li(1)

IS is the isomeric chemical shift with respect to α-Fe, QS is the quadrupole splitting, *W* is the absorption line width, *A* fraction population of a position with iron, V_{zz} is the electric field gradient, and *e* is the electron charge.

The application of the EPR method to study the $LiCuFe_2(VO_4)_3$ compound with the howardevansite structure made it possible to find the Landé splitting factor g = 2.005. The *g*-factor close to 2 indicated that

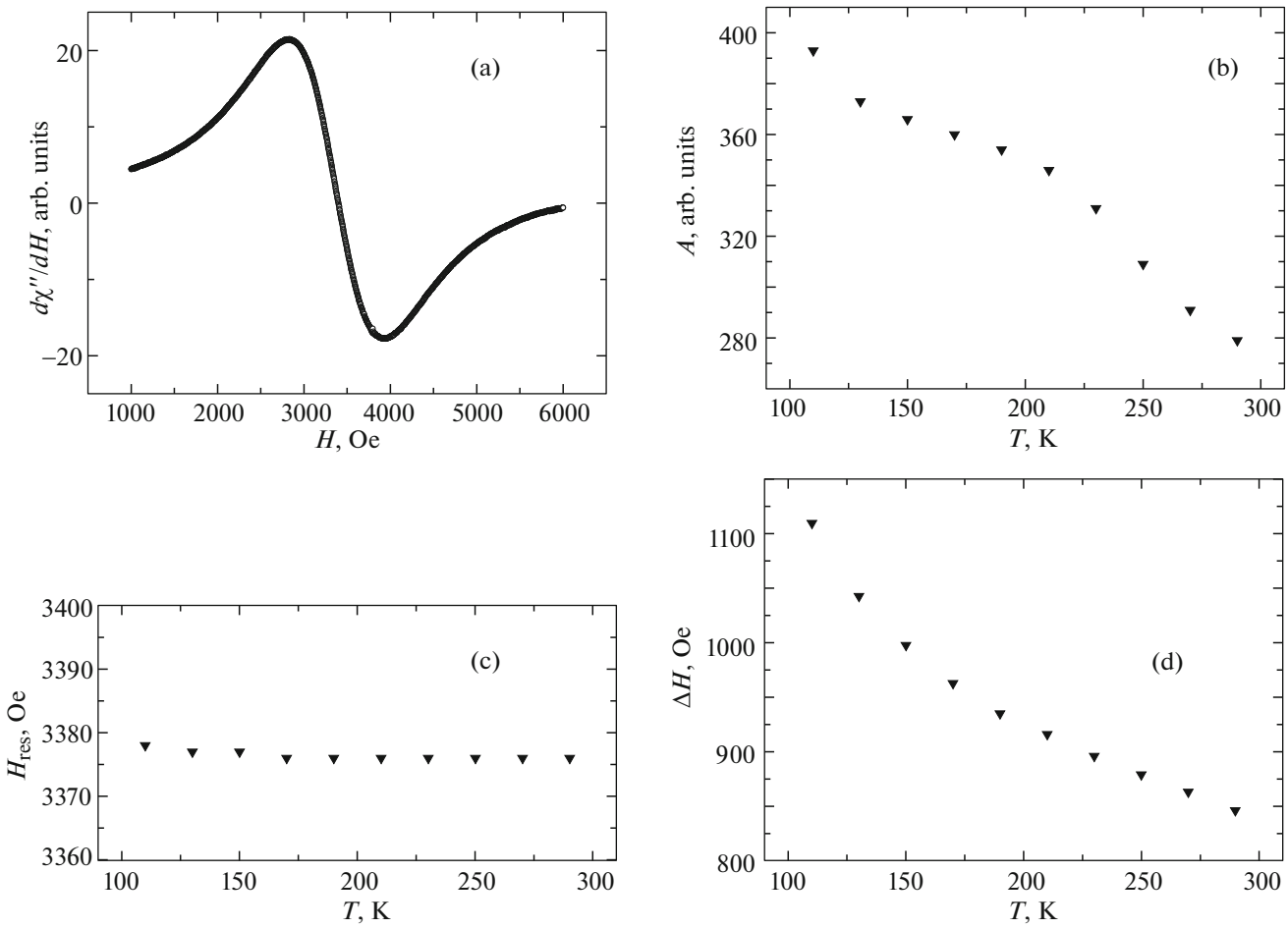

Fig. 4. (a) EPR spectrum of $LiCuFe_2(VO_4)_3$ measured in the *X* diapason at room temperature; the temperature dependences of the EPR-signal parameters in the $LiCuFe_2(VO_4)_3$ sample: (b) amplitude, (c) resonance field, and (d) line width.

the observed resonance line corresponded to a signal from ions with purely spin moment ($L = 0$), which is characteristic of trivalent iron ions.

3.3. Results of Magnetic Measurements and an Analysis of Exchange Interactions in the $LiCuFe_2(VO_4)_3$ Compound

It is interesting to study the static magnetic properties of the $LiCuFe_2(VO_4)_3$ polyvanadate. Figure 5a shows the experimental temperature dependence of magnetic moment $M(T)$ of the $LiCuFe_2(VO_4)_3$ compound measured in magnetic field 0.05 T on the sample cooled to a temperature of 4 K in a zero magnetic field. The study of the specific features of the magnetization of the $LiCuFe_2(VO_4)_3$ compound showed that the change in the cooling the sample (cooling in a zero magnetic field and that in magnetic field 0.05 T) did not influence temperature dependence $M(T)$. It is seen that at low temperature, the temperature dependence of the magnetic moment at temperature T_{max} = 9.6 K had an anomaly that was likely to demonstrate the magnetic phase transition from the paramagnetic state to the state with long-range magnetic order at temperature T_N = 7 K (Fig. 5a). The existence of a wide maximum in the temperature dependence of the magnetic moment (ratio $T_N/T_{max} = 0.73 < 1$) made it possible to assume that magnetic structure forming at low temperatures in the $LiCuFe_2(VO_4)_3$ compound had a low-dimensional character.

Figure 5b shows the dependence of the inverse magnetic susceptibility χ^{-1} on temperature in magnetic field $H = 0.05$ T for the $LiCuFe_2(VO_4)_3$ vanadate. The study of dependence $\chi^{-1}(T)$ showed that it could be described by the Curie–Weiss law at high temperatures ($T > 50$ K). The asymptotic Néel temperature that is determined as an intersection point of axis T with the asymptote to curve $\chi^{-1}(T)$ had a negative value ($\Theta = -81$ K) and demonstrated predominantly antiferromagnetic exchange interactions in a complex magnetic subsystem of the sample that was formed by magnetic iron and copper ions.

The Curie–Weiss constant C = 0.0176 K found experimentally corresponded to the effective magnetic

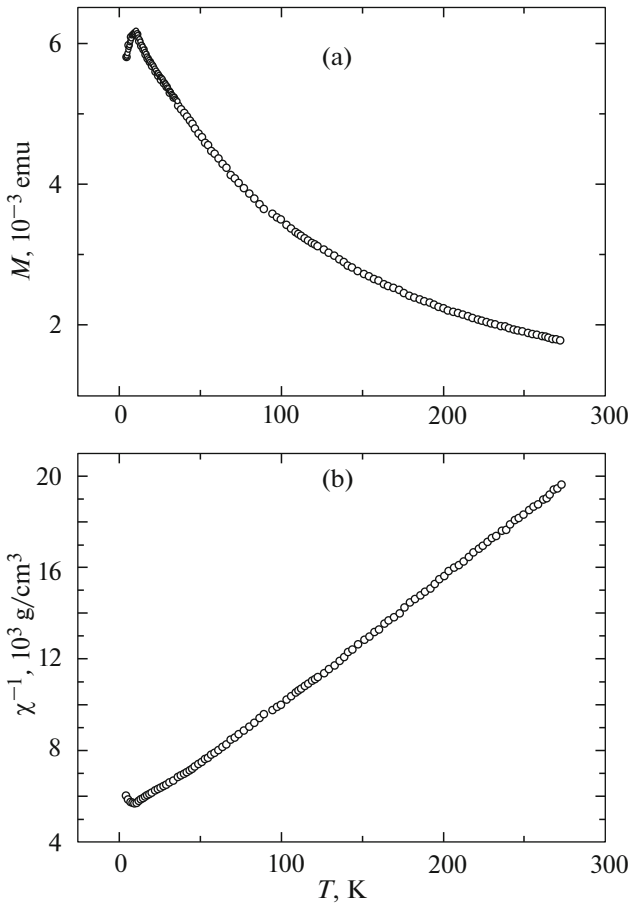

Fig. 5. Temperature dependences of (a) the magnetic moment and (b) the inverse magnetic susceptibility of $LiCuFe_2(VO_4)_3$ measured in magnetic field $H = 0.05$ T; the sample mass was $m = 0.07$ g.

moment (molar value) $\mu_{eff(exp)} = 8.6\mu_B$. The calculated effective magnetic moment of the $LiCuFe_2(VO_4)_3$ formula unit was $\mu_{eff(calc)} = 8.5\mu_B$ ($\mu_{eff(calc)}^{Fe^{3+}} = 5.91\mu_B$ and $\mu_{eff(calc)}^{Cu^{2+}} = 1.73\mu_B$).

According to [9, 10], the level of magnetic frustrations f in the sample can be estimated using relationship $|\Theta|/T_c = f$, where T_c ($\equiv T_N$) is the critical temperature below of which the magnetic order is stated. For the $LiCuFe_2(VO_4)_3$ compound, index $f \approx 12$ and corresponds to a high frustration level. Note that a nonfrustrated antiferromagnet has a typical value of $|\Theta|/T_c =$ 2–4.5 [10].

In this context, it is interesting to analyze the exchange couplings and magnetic interactions in the $LiCuFe_2(VO_4)_3$ compound. The magnetic subsystem of the sample is formed, first, by Fe^{3+} magnetic ions (electron configuration is $3d^5$, spin $S = 5/2$) existing in two nonequivalent crystallographic positions with the octahedral oxygen environment and, second, by Cu^{2+} magnetic ions (electron configuration is $3d^9$, spin $S =$ 1/2) which occupy the CuO_5 trigonal bipyramids. The spin configuration determined by the combination of exchange interactions in the sample corresponds to the minimum of the magnetic system energy. Consider the exchange interactions in $LiCuFe_2(VO_4)_3$ in terms of a simple model of indirect coupling [11, 12]. The model makes it possible to qualitatively estimate absolute values of the exchange integral and to describe the relation between the intersublattice interactions. Two types of the exchange interactions can be separated in an approximation of the nearest neighboring atoms. The interactions inside the zigzag-shaped chains are occurred via short indirect Fe–O–Fe and Fe–O–Cu bonds. The interchain interactions occur via extended Fe–O–V–O–Fe, Fe–O–V–O–Cu, and Cu–O–V–O–Cu. The intra chain interactions are described by integrals

$$J(\text{Fe–Fe}) = -\frac{4}{25}c\left(\frac{8}{3}b + c\right)U_{Fe}, \quad (1)$$

$$J(\text{Fe–Cu}) = -\frac{1}{5}c[b(U_{Fe} + U_{Cu})] - \left(\frac{13}{3}b + 2c\right)J^{in}. \quad (2)$$

The interchain interactions are described by integrals

$$J(\text{Fe–V–Fe}) = -\frac{4}{25}a^2\left(\frac{8}{9}b^2 + c^2\right)(U_{Fe} + U_{Cu}) \times \cos\theta_1\cos\theta_2, \quad (3)$$

$$J'(\text{Fe–V–Fe}) = -\frac{2}{5}a^2\left(\frac{8}{9}b^2(U_{Fe} + 2U_V + U_{Cu}) - c^2J^{in}\right)\times\cos\theta_1\cos\theta_2, \quad (4)$$

$$J''(\text{Fe–V–Cu}) = -\frac{1}{5}a^2\left[\frac{4}{9}b^2(U_{Fe} + 2U_V + U_{Cu}) - (b^2 + 2c^2)J^{in}\right]\cos\theta_1\cos\theta_2, \quad (5)$$

$$J'(\text{Cu–V–Cu}) = -\frac{32}{9}a^2b^2(U_{Cu} + U_V)\cos\theta_1\cos\theta_2, \quad (6)$$

$$J''(\text{Cu–V–Cu}) = -\frac{2}{3}a^2b^2\left[\frac{1}{3}(U_{Cu} + U_V) - J^{in}\right] \times\cos\theta_1\cos\theta_2. \quad (7)$$

Note that we have two equations (4) and (5) and two equations (6) and (7) for interchain exchange integrals J' and J'', relatively, which describe the Fe–V–Cu and Cu–V–Cu interactions. They are provided by different mutual orientation of principal axes of ligand polyhedrons containing interacting cations. The expressions for the exchange integrals contain the following denotations: a is the parameter of the ligand–cation electron transfer in the VO_4 tetrahedron, b is the parameter of the ligand–cation electron transfer over the σ bond in octahedra and bipyramids, c is the parameter of the ligand–cation electron transfer over the π bond (these parameters are squares of the stirring parameters in expressions of binding molecular orbit-

Table 4. Calculated integrals of intersublattice exchange interactions and exchange fields in $LiCuFe_2(VO_4)_3$ (the values corresponding to the ordering exchange interactions are shown by the bold type; the values corresponding to the disordering (frustrating) exchange interactions are shown by the italic type; the relative orientation of the cation magnetic moments is indicated by arrows)

Magnetic sublattice	Fe(1)↑		Fe(1)↓		Fe(2)↑		Fe(2)↓		Cu↑		Cu↓		H_e^+, K	H_e^-, K
	J^{intra}, K	J^{inter}, K	J^{intra}, K	J^{inter}, K	J^{intra}, K	J^{inter}, K	J^{intra}, K	J^{inter}, K	J^{intra}, K	J^{inter}, K	J^{intra}, K	J^{inter}, K		
Fe(1)↑	0	*−0.04*	**−4.94**	**−0.03**	0	*−0.10*	0	**−0.11**	0	*−0.17*	**−0.70**	**−0.09**	**13.09**	*0.44*
Fe(1)↓	**−4.94**	**−0.03**	0	*−0.04*	0	**−0.11**	0	*−0.10*	**−0.70**	**−0.09**	0	*−0.17*	**13.09**	*0.44*
Fe(2)↑	0	*−0.11*	0	**−0.13**	0	*−0.08*	**−4.94**	**−0.05**	0	*−0.40*	**−0.70**	**−0.19**	**13.24**	*0.68*
Fe(2)↓	0	**−0.13**	0	*−0.11*	**−4.94**	**−0.05**	0	*−0.08*	**−0.70**	**−0.19**	0	*−0.40*	**13.24**	*0.68*
Cu↑	0	*−0.17*	**−0.70**	**−0.09**	0	*−0.40*	**−0.70**	**−0.19**	0	*−1.16*	0	**−0.85**	**4.37**	*2.00*
Cu↓	**−0.70**	**−0.09**	0	*−0.17*	**−0.70**	**−0.19**	0	*−0.40*	0	**−0.85**	0	*−1.16*	**4.37**	*2.00*

als), U_{Fe}, U_{Cu}, and U_V are the energy of the ligand–cation electronic excitation for corresponding cations; J^{in} is the integral of intraatomic interaction (the Hund integral) for Cu^{2+}, and $\cos\theta_1$ and $\cos\theta_2$ are used to describe the angular dependence of the exchange interaction parameters.

Using the covalence parameters for simple oxides $U_V = 7$ eV, $U_{Fe} = 4.2$ eV, $U_{Cu} = 2.3$ eV, $J^{in} = 1.5$ eV, $a = 0.09$, $b = 0.02$, and $c = 0.01$ [13, 14], we can estimate the values of cation–cation indirect exchange interactions. The values of the exchange interaction constants are substantially in magnitudes for various cation pairs and kinds of intermediate ions. Thus, breaking the magnetic system of $LiCuFe_2(VO_4)_3$ into six sublattices, we note that the relatively strong negative intrachain interactions form an antiferromagnetic spin chain elongated along the **b**–**c** direction, and the relatively weak interchain interactions form a three-dimensional magnetic system. With allowance for the numbers of indirect bonds z_{ij}, the calculated values of the intersublattice exchange interactions $\sum z_{ij}J_{ij}$ are given in Table 4, in which the intrachain exchange interactions J^{intra} and the interchain exchange interactions J^{inter} are given in individual columns. Two last columns of Table 4 contain positive H_e^+ and negative H_e^- contributions to the exchange field that acts on each sublattice site. Thus, Table 4 illustrates the relation between the inter- and intrasublattice interactions and the tendency of the magnetic moment to be oriented each to other.

An analysis of the exchange interactions shows that the resulting interchain interactions are disordering for all cations of this compound: –0.08 K for Fe(1), –0.22 K for Fe(2), and –0.60 K for Cu.

Thus, in terms of the indirect bond model, the $LiCuFe_2(VO_4)_3$ compound is an antiferromagnetic with strong intrachain and frustrating interchain exchange interactions. This relation between the exchange interactions in the magnetic system of the sample causes significant difference between the magnetic and paramagnetic Néel temperatures. The magnetic structure denoted in Table 4 by arrows was dedicated in a collinear approximation. According to the Yafet–Kittel theory [15], magnetic moments of a strong sublattice can undergo an angularity leading to the triangular ordering when the ratio of the intrasublattice to interlattice interactions is higher than the ratio of the sublattice magnetizations. The system can return to the collinear antiferromagnetic ordering with further increasing the frustrating interactions. It is possible that, in view of strong frustrating effects, we are dealing exactly with such a situation. Thus, the real magnetic structure is dependent on not only the ratio of intra- and intersublattice interactions, but also the ratio of the magnetic moments of the sublattices, the cation distribution, and the degree of cation ordering over the crystallographic positions. The degree of low-dimensionality introduces certain contribution to the magnetic behavior.

4. CONCLUSIONS

The $LiCuFe_2(VO_4)_3$ compound was synthesized by a solid-phase reaction method. The X-ray diffraction confirmed the phase purity of the samples produced.

The complex study of the structural, static magnetic, and resonance properties of polyvadanate $LiCuFe_2(VO_4)_3$ made it possible to characterize the compound and to make the following conclusions.

The crystal symmetry of $LiCuFe_2(VO_4)_3$ is described by triclinic space group $P\bar{1}$. The unit cell parameters are as follows: $a = 8.1489(2)$ Å, $b = 9.8047(2)$ Å, $c = 6.6341(1)$ Å, $\alpha = 103.811(2)°$, $\beta = 102.370(2)°$, $\gamma = 106.975(2)°$. The unit cell contains two formula units, which agrees with the X-ray diffraction data from [6].

The study of the magnetic properties of oxide $LiCuFe_2(VO_4)_3$ showed that this compound was a paramagnetic with the effective magnetic moment $\mu_{eff(exp)} = 8.6\mu_B$ a temperatures higher than Néel temperature $T_N = 7$ K. At high temperatures ($T > 50$ K),

the paramagnetic susceptibility followed the Curie–Weiss law with the asymptotic Néel temperature $\Theta = -81$ K. The negative value of Θ indicated the predominant role of the antiferromagnetic exchange interactions in the magnetic system of the $LiCuFe_2(VO_4)_3$ sample. Based on the abovementioned, we can note that $LiCuFe_2(VO_4)_3$ is a quasi-low-dimensional magnet. Below the Néel temperature, the sample was in a magnetically ordered state that was determined by the competition between the exchange interaction with high index of magnetic frustration $f \approx 12$.

As a result of the gamma-resonance measurements, it was found that the principal iron positions in polyvanadate $LiCuFe_2(VO_4)_3$ had chemical shifts IS = 0.380 and 0.381 mm/s with respect to α-Fe and quadrupole splitting QS = 0.55 and 0.75 mm/s. These parameters correspond to the trivalent iron cations that are in the octahedral environment of oxygen ions. Note that these results agree with the X-ray diffraction data.

It was found that the EPR signal observed in the paramagnetic range of oxide $LiCuFe_2(VO_4)_3$ contained one absorption line with the Landé splitting factor $g = 2$ that is characteristic of Fe^{3+} ions. Thus, The EPR spectrum showed that the magnetic properties of the $LiCuFe_2(VO_4)_3$ compound were mainly determined by Fe^{3+} ions.

The estimation of the exchange interactions in terms of the indirect bond model led to the conclusion that $LiCuFe_2(VO_4)_3$ was an antiferromagnet with relatively strong antiferromagnetic intrachain and frustrating interchain interactions. The neutron scattering experiments could verify the adequacy of these conclusions.

REFERENCES

1. C. Castelnovo, R. Moessner, and S. L. Sondhi, Nature (London) **451**, 42 (2008).
2. S. S. Sosin, L. A. Prozorova, and A. I. Smirnov, Phys.—Usp. **48** (1), 83 (2005).
3. S. T. Bramwell and M. J. P. Gingras, Science (Washington) **294**, 1495 (2001).
4. J. Snyder, B. G. Ueland, J. S. Slusky, H. Karunadasa, R. J. Cava, and P. Schiffer, Phys. Rev. B: Condens. Matter **69**, 064414 (2004).
5. H. Kadowaki, N. Doi, Y. Aoki, Y. Tabata, T. J. Sato, J. W. Lynn, K. Matsuhira, and Z. Hiroi, J. Phys. Soc. Jpn. **78**, 103706 (2009).
6. A. A. Belik, Mater. Res. Bull. **34** (12), 1973 (1999).
7. D. A. Velikanov, Vestn. Sib. Gos. Aerokosm. Univ, No. 2, 176 (2013).
8. *Bruker AXS TOPAS V4. General Profile and Structure Analysis Software for Powder Diffraction Data: User's Manual* (Bruker AXS, Karlsruhe, Germany, 2008).
9. J. E. Greedan and A. P. Ramirez, Comments Condens. Matter Phys. **18**, 21 (1996).
10. J. E. Greedan, J. Mater. Chem. **11**, 37 (2000).
11. P. W. Anderson, Phys. Rev. **115** (1), 1 (1959).
12. M. V. Eremin, in *Spectroscopy of Crystals* (Nauka, Leningrad, 1985), pp. 150–171 [in Russian].
13. O. A. Bayukov and A. F. Savitskii, Phys. Solid State **36** (7), 1049 (1994).
14. O. A. Bayukov and A. F. Savitskii, Phys. Status Solidi B **155** (2), 249 (1989).
15. S. Krupicka, *Physik der Ferrite und der verwandten magnetischen Oxide* (Academia, Prague, 1973; Mir, Moscow, 1976), Vol. 1 [in German and in Russian].

Translated by Yu. Ryzhkov